Inorganic Chemistry

pubs.acs.org/IC
Article

Understanding Pressure Effects on Structural, Optical, and Magnetic Properties of $CsMnF_4$ and Other $3d^n$ Compounds

Guillermo Santamaría,[†] Toraya Fernández-Ruiz,*[,†] Juan María García-Lastra, Pablo García-Fernández, Inés Sánchez-Movellán, Miguel Moreno, and José Antonio Aramburu

Cite This: *Inorg. Chem.* 2024, 63, 13231−13243

ABSTRACT: The pressure dependence of structural, optical, and magnetic properties of the layered compound $CsMnF_4$ are explored through first-principles calculations. The structure at ambient pressure does not arise from a Jahn−Teller effect but from an orthorhombic instability on MnF_6^{3-} units in the tetragonal parent phase, while there is a $P4/n \rightarrow P4$ structural phase transition at $P = 40$ GPa discarding a spin crossover transition from $S = 2$ to $S = 1$. The present results reasonably explain the evolution of spin-allowed d−d transitions under pressure, showing that the first transition undergoes a red-shift under pressure following the orthorhombic distortion in the layer plane. The energy of such a transition at zero pressure is nearly twice that observed in Na_3MnF_6 due to the internal electric field and the orthorhombic distortion also involved in K_2CuF_4. The reasons for the lack of orthorhombic distortion in K_2MF_4 (M = Ni, Mn) or $CsFeF_4$ are also discussed in detail. The present calculations confirm the ferromagnetic ordering of layers in $CsMnF_4$ at zero pressure and predict a shift to an antiferromagnetic phase for pressures above 15 GPa consistent with the reduction of the orthorhombicity of the MnF_6^{3-} units. This study underlines the usefulness of first-principles calculations for a right interpretation of experimental findings.

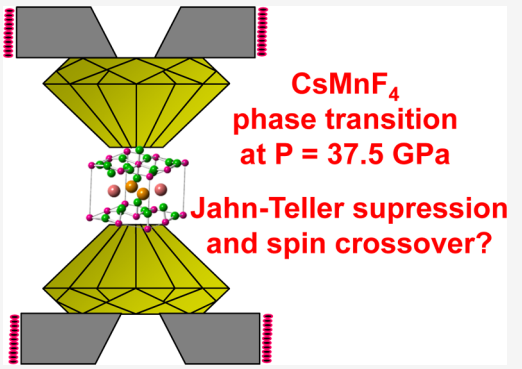

INTRODUCTION

Insulating transition metal (TM) compounds are an important family of materials characterized by the presence of localized d electrons with strong correlation, giving rise to the interplay of electronic, charge, spin, and orbital degrees of freedom. These compounds are involved in a number of technological applications such as solid-state lasers,[1−3] devices with colossal magnetoresistance,[4] or solar cells[5] and in their understanding appear concepts like orbital ordering, superexchange, or vibronic instabilities.[6−9]

Due to the open shell structure of the cation, TM compounds usually exhibit optical response in the V−UV domain and magnetic ordering, and thus, optical and magnetic tools are widely used in their characterization. In this realm the application of high pressures on a TM compound opens a new window for detecting attractive phenomena such as phase transitions or changes in electronic states of TM complexes where active electrons are localized.[10−15] In particular, pressure can change the ground-state spin of a complex shifting from a high- to a low-spin configuration[10] such as happens for a variety of Fe^{2+} complexes.[16]

To understand optical data under pressure, it is crucial to know the evolution of interatomic distances and the nature of involved optical transitions. This requirement is however more difficult to fulfill when the TM complex is distorted from octahedral symmetry. As both conditions are often not fulfilled, first-principles calculations can be of help for gaining the right insight into this matter. Furthermore, in high-pressure experiments optical spectra are sometimes only recorded at room temperature[12,17] where the resolution is certainly poorer than at 4.2 K, and thus, theoretical calculations can aid to overcome that hindrance as well.

This work is devoted, in a first step, to understand the optical absorption spectra under pressure of $CsMnF_4$.[17] This compound belongs to the interesting family of fluoromanganates[18−20] with formula $AMnF_4$ (A = alkali monocation or NH_4^+) involving the $3d^4$ cation Mn^{3+}. This family has deserved much attention as a model to correlate the various structural, magnetic, and optical properties, both at ambient pressure (study of the chemical pressure effects linked to the change of monocation A) and under high hydrostatic pressure. Among these layered compounds the most studied system is just $CsMnF_4$ as it is the only one with a tetragonal structure and ferromagnetic (FM) order in the layer planes at ambient pressure when $T < T_c = 23$ K.[19]

Received: February 13, 2024
Revised: June 10, 2024
Accepted: June 12, 2024
Published: July 10, 2024

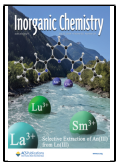

https://doi.org/10.1021/acs.inorgchem.4c00599
Inorg. Chem. 2024, 63, 13231−13243

According to X-ray diffraction data by Molinier and Massa, $CsMnF_4$ at ambient pressure belongs to the $P4/n$ space group.[18] The structure is depicted in Figure 1 showing that

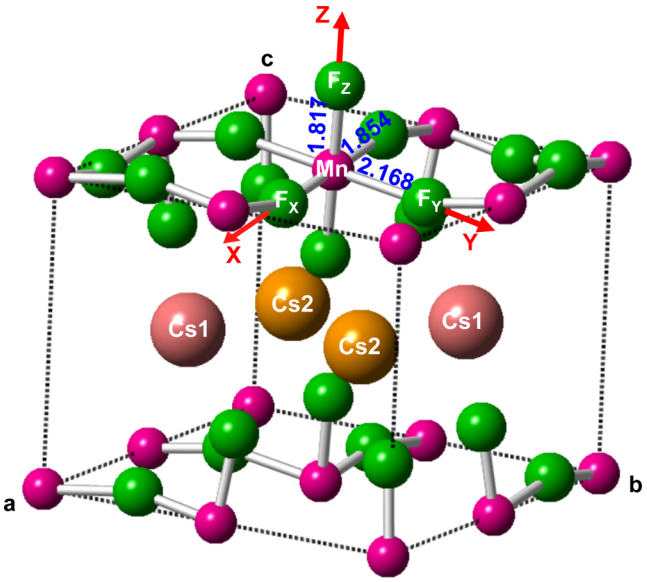

Figure 1. Experimental unit cell of the $CsMnF_4$ structure corresponding to the $P4/n$ phase at $P = 0$. Red arrows indicate the local {X, Y, and Z} axes of a MnF_6^{3-} complex. Blue numbers indicate the Mn−F distances (in Å). The lattice parameters are $a = b = 7.944$ Å and $c = 6.338$ Å.

Mn^{3+} ions are disposed in layers in the ab plane although the F^- ions of MnF_6^{3-} units are not strictly in that plane just reflecting the existence of buckling. In the involved MnF_6^{3-} units the shortest Mn−F distance corresponds to the z direction, perpendicular to the ab layer plane ($R_z = 1.817$ Å), while the longest one ($R_y = 2.168$ Å) is nearly perpendicular to the z direction. The last Mn−F distance ($R_x = 1.854$ Å) differs from that of R_z by only 0.037 Å.

Interestingly, the F−Mn−F angle of MnF_6^{3-} units in $CsMnF_4$ differs by less than 3° from 90°. This fact and a Mn−F−Mn angle of 162°, a consequence of buckling, leads to a local symmetry around a Mn^{3+} ion that is not strictly orthorhombic (D_{2h}) but C_i. $CsMnF_4$ exhibits an antiferrodistortive arrangement and thus in two adjacent MnF_6^{3-} units that share a common ligand the longest axes are essentially perpendicular. The $RbMnF_4$ and $KMnF_4$ compounds of the $AMnF_4$ family also involve puckered layers but do not belong to the $P4/n$ space group and have a Mn−F−Mn angle equal to 148° and 140°, respectively.[18,19] Both compounds are antiferromagnetic but only below 5 K.[19,20]

In the interpretation of structural and optical data (Figure 2) of $CsMnF_4$ there are two relevant questions that need to be clarified: (1) The local distortion of MnF_6^{3-} units in $CsMnF_4$ has usually been ascribed to the Jahn−Teller effect[17−21] despite the low symmetry of the compound. (2) From the optical absorption data under pressure (Figure 2) it has been proposed that the ground state of MnF_6^{3-} units in $CsMnF_4$ undergoes a spin crossover transition from $S = 2$ to $S = 1$ for a pressure around 38 GPa.[17] As these kinds of transitions have been observed for complexes with ligands such as CN^- or SCN^-[10,16] its possible existence for a fluoride complex certainly deserves a further investigation. For achieving this goal, the lack of data on the evolution of Mn−F distances

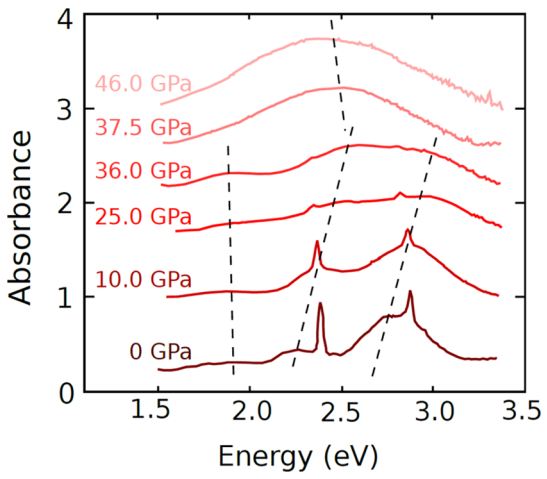

Figure 2. Experimental optical spectra of $CsMnF_4$ in the 1.5−3.5 eV range measured at room temperature for zero pressure and also P = 10.0, 25.5, 36.0, 37.5, and 46.0 GPa, (adapted from ref 17). Dotted lines are the approximate variations in the energies of the band maxima as proposed in ref 17, although this proposal is discussed in the text.

under pressure for $CsMnF_4$ hampers the interpretation of optical absorption results, a circumstance that can, however, be overcome by means of theoretical calculations.

Finally, the present work also pays attention to the ferromagnetism displayed by $CsMnF_4$ at zero pressure, as well as the evolution of the magnetic order under an applied pressure. At this point, the recent results derived for insulating layered compounds like K_2CuF_4 or Cs_2AgF_4 shed light on that issue.[9,22,23]

This work is organized as follows. The computational tools employed in this work are briefly described in the next section, and we then discuss the previous interpretations of experimental data on $CsMnF_4$ together with the main results obtained in this work. Some final remarks are reported in the last section.

COMPUTATIONAL TOOLS

First-principles density functional theory (DFT) calculations (performed using hybrid exchange−correlation functionals) were conducted to analyze the influence of the pressure on the geometry, magnetic order, and optical transitions of the layered compound $CsMnF_4$. In order to be sure of the calculated properties, we have used two codes, Crystal17 and VASP, with different implementations of the DFT for periodic crystals, obtaining very similar results.

On the one hand, the Crystal17 code[24] has two relevant implementations, significantly speeding up the calculations: first, it makes full use of the symmetries of the material's space group, and second, Bloch orbitals are represented through linear combinations of Gaussian type functions.[25−27] On the other hand, Vienna Ab initio Simulation Package (VASP)[28,29] employs a set of plane waves to describe the Bloch orbitals, enabling highly accurate results in reproducing experimental geometries in all kinds of compounds, including organic and hybrid organic−inorganic materials.[30−33]

First, we optimized with the Crystal17 code the geometry of $CsMnF_4$ at the experimental $P4/n$ phase[18] using different magnetic phases, obtaining the minimum energy for the experimental FM order with values of both lattice parameters

https://doi.org/10.1021/acs.inorgchem.4c00599
Inorg. Chem. 2024, 63, 13231−13243

and bond Mn−F distances similar to the experimental data, with discrepancies of less than 3.5%. The next step was the acquisition of the parent phase of the experimental $CsMnF_4$ $P4/n$ structure. For this goal we started from the experimental $CsMnF_4$ structure substituting all open shell Mn^{3+} ions, with d^4 electronic configuration and $S = 2$, by Fe^{3+} ions (d^5 electronic configuration and $S = 5/2$) with spherical density (in vacuo) and equal ionic radius, $r(Mn^{3+}) \approx r(Fe^{3+}) \approx 0.785$ Å.[34] The symmetry of the optimized $CsFeF_4$ parent phase was $P4/nmm$, precisely the experimental phase of this compound.[35] Moreover, in order to elucidate the nature of the phase transition experimentally observed in $CsMnF_4$ under a pressure $P \approx 38$ GPa,[17] we have also optimized the structure of this compound under hydrostatic pressures in the range of $P = 0-60$ GPa. Furthermore, for each optimized structure, we have followed the unstable harmonic modes in the supercell and found the corresponding ground state.

Geometry optimizations under pressure from 0 to 60 GPa, in 10 GPa increments, were also performed with the VASP code using initial geometries provided by the Crystal17 optimizations, significantly expediting the VASP convergence process.

Energies of the d−d optical transitions were calculated for each optimized geometry under pressure. For the Crystal17 optimized geometries, DFT calculations have been carried out on MnF_6^{3-} complexes by means of the Amsterdam density functional (ADF) code.[36,37] In these pseudomolecular calculations, the MnF_6^{3-} clusters were embedded in the electrostatic potential of the rest of lattice ions,[38] which was previously calculated through Ewald−Evjen summations.[39,40]

In a different strategy, we have also calculated the energy values of these d−d transitions with VASP, using a different embedding by substituting three of the four Mn^{3+} atoms in the unit cell with Ga^{3+}, atoms with a d^{10} configuration, and thus a symmetric electron density. The energies of the optical transitions were determined for each pressure ranging from 0 to 60 GPa, by using the ΔSCF method.[41,42] The ΔSCF method consists of a self-consistent calculation of the total energy for the ground state, yielding the corresponding E_{GS}. The geometries used are the ones obtained from the optimization of the periodic $CsMnF_4$ system. At the same geometry the electronic configuration of an excited state is imposed by manually adjusting the occupations of the d-like Kohn−Sham orbitals, and the SCF procedure is performed again, to obtain the corresponding E_{exc} energy. The energy difference, $E_{exc} - E_{GS}$, is taken as the electronic transition energy. Results of these calculations are very similar to the ones performed by means of the ADF code.

More details on the calculations with both codes can be found in the Supporting Information.

ANALYSIS OF PREVIOUS INTERPRETATIONS OF STRUCTURAL AND OPTICAL DATA FOR $CSMNF_4$

The optical properties in the V−UV domain of an insulating compounds like $CsMnF_4$ greatly depend on the involved MnF_6^{3-} units, whose ground state in O_h symmetry can, in principle, be either $^5E_g(t^3e^1)$ or $^3T_{1g}(t^4e^0)$.[43] Nevertheless, experimental data, at ambient pressure, on compounds containing MnF_6^{3-} support a high-spin configuration ($S = 2$) as ground state.[12,19,20] Octahedral complexes with inorganic ligands like F^- or Cl^- display a high-spin configuration for $3d^n$ ions ($n = 5, 6$) like Fe^{3+} or Fe^{2+} while a low-spin configuration is found for complexes of 4d and 5d ions, like Ru^{3+} or Ir^{4+}, involving higher 10Dq values.[10,44] A low-spin ($S = 1/2$) ground state has also been reported[45,46] for NiF_6^{3-} complexes in A_3NiF_6, Cs_2ANiF_6 (A = Na, K), and Rb_2NaNiF_6 fluorides and also in oxides doped with Ni^{3+}.[47] However, electron paramagnetic resonance (EPR) measurements carried out in Ni^{3+}-doped $KMgF_3$ and $CsCaF_3$ perovskites[48,49] lead to a high-spin ($S = 3/2$) ground state. These results show that, in NiF_6^{3-} complexes, the high-spin/low-spin energy separation must be very small.[45,46] Moreover, magnetic measurements performed on Li_3NiF_6 characterized at low temperature a low-spin configuration ($S = 1/2$), which tends to a high-spin one with increasing temperature.[50] To the best of our knowledge, a spin crossover under pressure in fluorides containing NiF_6^{3-} complexes has not been found.

As in 6-fold coordinated compounds of d^4 ions (Mn^{3+}, Cr^{2+}), the local symmetry of a MnF_6^{3-} complex corresponds to a distorted octahedron, and the ground state wave function, Ψ_g, can briefly be written as

$$\Psi_g(S = 2; M_s = 2) = |t_1 \uparrow\ t_2 \uparrow\ t_3 \uparrow\ e_1 \uparrow| \quad (1)$$

Here the three t_i ($i = 1, 2, 3$) and e_j ($j = 1, 2$) orbitals come from the $t_{2g}(xz, xy, yz)$ and $e_g(3z^2-r^2, x^2-y^2)$ orbitals in O_h symmetry, and thus, the e_2 orbital is empty in the ground state.[13] Accordingly, the spin-allowed transitions ($\Delta S = 0$) are simply described by $t_i\uparrow \rightarrow e_2\uparrow$ ($i = 1, 2, 3$) and $e_1\uparrow \rightarrow e_2\uparrow$. As the $e_1\uparrow \rightarrow e_2\uparrow$ transition is usually the lowest, its energy is termed E_0 while those associated with the $t_i\uparrow \rightarrow e_2\uparrow$ transitions are simply called E_i ($i = 1, 2$, and 3). In addition to the spin-allowed transitions, sharp peaks with smaller oscillator strengths associated with forbidden transitions ($\Delta S = -1$) are sometimes observed in optical spectra of d^4 ions (Mn^{3+}, Cr^{2+}). They correspond to excited states with $S = 1$ and are described by determinants like $|t_1\uparrow\ t_2\downarrow\ t_3\uparrow\ e_1\uparrow|$ so the total spin of the t-subshell is only 1/2. Such forbidden transitions have well been detected for CrF_2.[51] Similar transitions with $\Delta S = -1$ are also observed in the absorption spectra of CrO_6^{9-} or CrF_6^{3-} units and are little sensitive to pressure.[52,53,14,15]

Figure 2 reproduces the experimental optical absorption spectra at room temperature of $CsMnF_4$ in the 1.5−3.5 eV range for pressures up to 46 GPa.[17] The spectra for $P < 25$ GPa involve three poorly resolved broad bands and two sharp peaks that are little sensitive to pressure and progressively disappear at higher pressures. Accordingly, it is not easy to know from experimental results at ambient pressure (Figure 2) the number of spin-allowed transitions and the corresponding energies. In the pressure range 37.5−46.0 GPa only one broad band is observed in the optical spectrum of $CsMnF_4$ whose maximum is around 2.5 eV, and its bandwidth is higher than ∼1 eV. No signs of a structural phase transition around 1.4 GPa, early suggested by Moron et al.,[21] have been found in the optical measurements on $CsMnF_4$.

Seeking to understand the optical spectra of $CsMnF_4$ at ambient pressure it has been proposed that the experimental geometry of MnF_6^{3-} units is the result of a static Jahn−Teller (JT) effect.[17] Under that assumption, also followed in other works,[18−21] the JT effect would be responsible for having tetragonal MnF_6^{3-} units with Y as the local principal axis of the complex (Figure 1). Such units are elongated in accord with the geometry widely observed for systems actually displaying a static JT effect.[54−56] Consequently, e_1 would be a molecular orbital transforming like $3y^2-r^2$ while the unoccupied e_2 orbital corresponds to z^2-x^2. According to this hypothesis, the optical absorption spectrum of $CsMnF_4$ at ambient pressure would

https://doi.org/10.1021/acs.inorgchem.4c00599
Inorg. Chem. 2024, 63, 13231−13243

involve three spin-allowed transitions in the MnF_6^{3-} unit whose energies have been proposed[17] to be E_0 = 1.80 eV, E_1 = 2.26 eV, and $E_2 = E_3$ = 2.80 eV from Figure 2. Such values are close to E_0 = 1.92 eV, E_1 = 2.23 eV, and $E_2 = E_3$ = 2.73 eV reported by Morón and Palacio.[57]

Nonetheless, doubts are raised by the JT assumption due to the following reasons:[54−57,9]

(i) The existence of a JT effect requires a degenerate electronic state in the *initial* geometry. Therefore, as $CsMnF_4$ is a layered compound, even if the geometry of the initial parent phase is tetragonal the electronic ground state of an MnF_6^{3-} unit should not be degenerate according to symmetry.

(ii) $CsMnF_4$ is a layered compound where layers are perpendicular to the crystal **c** axis (Figure 1). Accordingly, one would expect that the axis of the MnF_6^{3-} unit perpendicular to the layer plane plays a singular role, a fact seemingly not consistent with the JT assumption.

(iii) The local equilibrium geometry for MnF_6^{3-} in $CsMnF_4$ is not tetragonal. Indeed, even assuming Y as the main axis (Figure 1) the symmetry would be at most orthorhombic because $R_X - R_Z$ = 0.037 Å. Accordingly, one should expect four and not only three d−d transitions with $\Delta S = 0$ for $CsMnF_4$.

(iv) Although most of the d^9 systems which exhibit a static JT effect are elongated with a hole in an x^2-y^2 type orbital[54−57] this is not a general rule. For instance, in the cubic CaO lattice doped with Ni^+, the hole is in a $3z^2-r^2$ orbital and the octahedron compressed.[58,59] In non-JT systems like $K_2ZnF_4:Cu^{2+}$, where the host lattice is tetragonal, the hole is also in $3z^2-r^2$.[60,61]

Looking at higher pressures, the optical spectrum of $CsMnF_4$ seems to undergo some change around 37 GPa as above this pressure the optical spectrum at room temperature involves only one very broad band (Figure 2). Such effect has been assumed to arise from a change of the ground-state configuration which would be $^3T_{1g}(t^4e^0)$ when P > 37 GPa with an O_h local geometry for MnF_6^{3-} units.[17]

No further arguments are given for underpinning that assumption that casts in principle some doubts. Indeed, just looking at Tanabe−Sugano diagrams[43] one would expect that in octahedral symmetry the transition of a $^5E_g(t^3e^1)$ ground state to $^3T_{1g}(t^4e^0)$ in MnF_6^{3-} takes place for 10Dq ≥ 3 eV. For estimating whether this condition is fulfilled, it is useful to consider that the 10Dq value derived from the four allowed transitions in Na_3MnF_6 (10Dq = 1.88 eV) is close to 10Dq measured for octahedral CrF_6^{3-} units in cubic elpasolites involving also a trivalent TM cation.[14,62,63] For instance, in the case of Rb_2KCrF_6, 10Dq = 1.97 eV at ambient pressure while a value d(10Dq)/dP = 0.014 eV/GPa has been measured in the range 0−10 GPa.[63] Accepting this value for a hypothetical O_h MnF_6^{3-} unit, one would expect 10Dq = 2.41 eV for P = 38 GPa. This figure is thus below 10Dq = 3 eV, which is the estimated value required for the spin crossover.

Given these facts, this work addresses the following questions centered on the interpretation of optical data under pressure in $CsMnF_4$: (1) the origin of the local geometry of MnF_6^{3-} units in $CsMnF_4$ and the nature of the electronic ground state at zero pressure; (2) the number and energies of the spin-allowed transitions at zero pressure and its evolution as a function of the applied pressure; and (3) the nature of the phase transition observed around 37 GPa, paying particular attention to a possible shift of the ground state spin from S = 2 to S = 1.

RESULTS AND DISCUSSION

Structure and Electronic Ground State at Zero Pressure. The calculated values of the lattice parameters and Mn−F distances of $CsMnF_4$ at zero pressure are collected in Table 1. Such values, derived using both CRYSTAL and VASP codes in a $P4/n$ space group, are compared to experimental findings.[18,19] As can be seen in Table 1 the differences between calculated and experimental values are always smaller than 1.5%. The electronic ground state of the MnF_6^{3-} unit is found to come from the $^5E_g(t^3e^1)$ configuration in cubic symmetry, thus implying a high-spin configuration with S = 2.

Table 1. Calculated Lattice Parameters and Mn−F Distances[a] for $CsMnF_4$ at Zero Pressure in the $P4/n$ Space Group Using VASP (First Row) and CRYSTAL (Second Row) Codes and Compared to Experimental Values[18,19]

	$a = b$	c	R_Z	R_X	R_Y
Experimental	7.944	6.338	1.817	1.854	2.168
Calculated	8.029	6.401	1.829	1.871	2.189
	7.961	6.347	1.818	1.877	2.161

[a]All distances are given in Å.

Seeking to understand the origin of the local structure in $CsMnF_4$, it is useful to analyze the evolution of the crystal structure when Mn^{3+} is replaced by a cation like Fe^{3+} with a similar ionic radius, giving rise to the so-called high-symmetry parent phase.[6,13,22,23] Under strict octahedral symmetry, Fe^{3+} in high-spin configuration (S = 5/2) exhibits a nearly spherical electronic density which is however never found for a $3d^4$ ion like Mn^{3+} or a $3d^9$ ion like Cu^{2+} in the same situation. After the $Mn^{3+} \rightarrow Fe^{3+}$ substitution, we carried out a geometry optimization of the $CsFeF_4$ structure maintaining fixed the experimental $P4/n$ space group of $CsMnF_4$. The obtained final structure has a higher symmetry belonging to the tetragonal $P4/nmm$ space group, although it still involves buckled layers (Table 2). It should be noted that the obtained local geometry of each FeF_6^{3-} unit in $CsFeF_4$ corresponds to a compressed octahedron with $R_X = R_Y$ and $R_Z < R_X$ (Table 2) and a symmetry practically tetragonal with Z as the main axis. Interestingly in the present case the calculated parent phase coincides with the experimental structure of the $CsFeF_4$ compound at normal conditions.[64,65] The calculated lattice parameters and Fe−F distances correspond to experimental ones within 1.5%.

Table 2. Calculated Lattice Parameters and Fe−F Distances for $CsFeF_4$ at Zero Pressure Assuming, in Principle, the $P4/n$ Space Group[a]

	$a = b$	c	R_Z	R_X	R_Y
Calculated	7.926	6.631	1.863	1.989	1.989
Experimental	7.787	6.540	1.884	1.959	1.959

[a]The results, derived through the CRYSTAL code, show that the system evolves until reaching the $P4/nmm$ space group, where $R_X = R_Y$ due to the higher symmetry. Experimental results[65] are given for comparison. All distances are given in Å.

https://doi.org/10.1021/acs.inorgchem.4c00599
Inorg. Chem. 2024, 63, 13231−13243

Bearing the preceding considerations in mind, we first consider $CsMnF_4$ in the tetragonal $P4/nmm$ geometry of the parent phase. In that case, the MnF_6^{3-} units are essentially tetragonal with R_Z = 1.80 Å and $R_X = R_Y$ = 2.011 Å. The main axis is Z, perpendicular to the layer plane, and the four antibonding valence orbitals are ordered as shown in Figure 3,

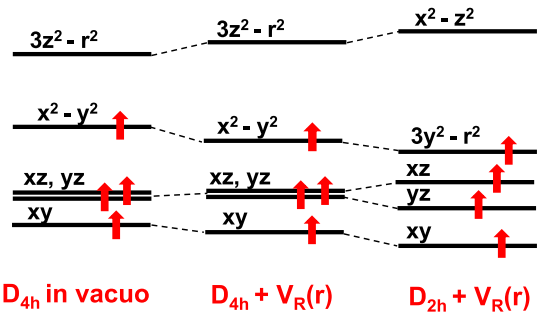

Figure 3. Qualitative scheme of the energy levels of the 5 antibonding orbitals with mainly d character of the MnF_6^{3-} complex in $CsMnF_4$ at zero pressure depicted in 3 steps: (1) complex in vacuo with D_{4h} geometry, (2) adding the internal $V_R(\mathbf{r})$ potential, and (3) in D_{2h} geometry and including the $V_R(\mathbf{r})$ potential.

giving rise to an orbitally singlet ground state. Following the compressed geometry, the LUMO corresponds to the molecular orbital of the MnF_6^{3-} unit transforming like $3z^2-r^2$ and is simply designated by $|3z^2-r^2\rangle$ while the highest occupied molecular orbital, HOMO, is $|x^2-y^2\rangle$. Accordingly, the ground state belongs to $^5A_{1g}$ in tetragonal symmetry and the $|x^2-y^2\rangle \rightarrow |3z^2-r^2\rangle$ excited state to $^5B_{1g}$.

At this point it is important to highlight that the gap, E_0, associated with the $|x^2-y^2\rangle \rightarrow |3z^2-r^2\rangle$ excitation in MnF_6^{3-} does not *only* reflect that in the parent phase $R_Z < R_X = R_Y$. Indeed, although active electrons are essentially localized in the MnF_6^{3-} unit they also feel the internal electric field, $E_R(\mathbf{r})$, due to ions of $CsMnF_4$ lying *outside* the complex, that gives rise to an extrinsic contribution to E_0 such as has been proved for layered compounds like K_2CuF_4 or La_2CuO_4[6,9,23,61,66]

Figure 4 depicts the electrostatic potential $V_R(\mathbf{r})$ associated with the internal field through $E_R(r) = -\nabla V_R(r)$. According to the shape of $(-e)V_R(\mathbf{r})$ it favors to increase the energy of $|3z^2-r^2\rangle$ and reduce that of $|x^2-y^2\rangle$, thus enhancing the value of E_0. We have derived a value E_0 = 0.7 eV considering only the isolated MnF_6^{3-} unit while E_0 = 1.2 eV is obtained once $V_R(\mathbf{r})$ is incorporated into the calculation. Therefore, $V_R(\mathbf{r})$ not only helps to stabilize $|x^2-y^2\rangle$ as HOMO but likely has a significant influence on optical transitions, a matter that will be discussed later.

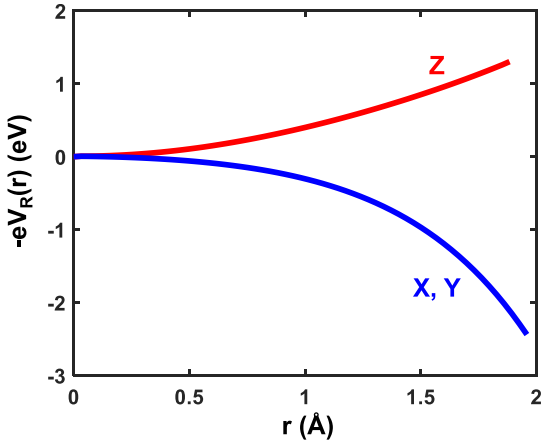

Figure 4. Potential energy $(-e)V_R(\mathbf{r})$ corresponding to the internal electric field created by the rest of the lattice ions of $CsMnF_4$ in the metastable $P4/nmm$ phase of $CsFeF_4$ on a MnF_6^{3-} complex. Energies are depicted along the local X, Y, and Z directions of the complex.

Interestingly, if $CsMnF_4$ is in the $P4/nmm$ phase the electronic density in the MnF_6^{3-} unit with an unpaired electron in $|x^2-y^2\rangle$ is compatible with a tetragonal symmetry ($R_Z < R_X = R_Y$) of the complex. This fact is thus consistent with the lack of JT effect under an *initial* tetragonal symmetry such as happens for K_2ZnF_4:Cu^{2+}.[61,76] Nevertheless, the equilibrium geometry of $CsMnF_4$ exhibits a lower $P4/n$ symmetry with $R_Y > R_X$ for the MnF_6^{3-} complex. This instability of the $P4/nmm$ structure for $CsMnF_4$ implies the existence of at least one vibration mode with imaginary frequency.[23] Accordingly, we have calculated the vibrational frequencies of $CsMnF_4$ in the optimized $P4/nmm$ geometry finding an a_{2g} lattice mode with a frequency equal to 367i cm^{-1}. The effect of that mode on the MnF_6^{3-} unit is described by the orthorhombic b_{1g} local mode (Figure 5) which is thus

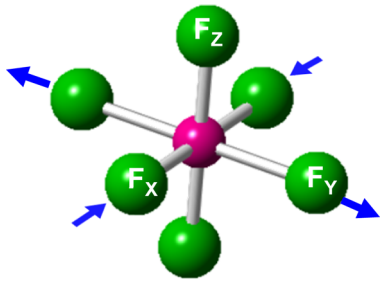

Figure 5. Picture of the local b_{1g} vibrational mode, which is unstable in $CsMnF_4$ in the parent phase $P4/nmm$ at P = 0.

responsible for having $R_Y - R_X$ = 0.31 Å in the final equilibrium geometry of $CsMnF_4$ at P = 0 (Table 1). The difference, ΔU, between the calculated energy per molecule for the equilibrium $P4/n$ and the parent $P4/nmm$ phase amounts to 71 meV and is thus the source for the orthorhombic instability shown in Figure 5. That instability, similar to that found for K_2CuF_4 or Cs_2AgF_4,[9,23] is driven by the electron–vibration coupling, H_{vib}, and involves changes in the ground state wave function and the associated electronic density.[8,67]

If H_0 denotes the Hamiltonian where all nuclei are frozen at a given position, the Hamiltonian H describing the small motions around it following the distortion coordinate Q of a nondegenerate mode can simply be written as

$$H = H_0 + H_{vib} = H_0 + V(r)Q + \ldots \quad (2)$$

It should be noted that H_{vib} exhibits the same symmetry as H_0 provided that symmetry operations are carried out on both electron and nuclei coordinates. Accordingly, in eq 2, V(r) transforms like the coordinate Q, and thus both operators belong to the same Γ irrep. If $\Psi_g(r)$ is the wave function of the ground-state orbital singlet then $\langle\Psi_g(r)|\ V(r)|\ \Psi_g(r)\rangle = 0$ unless Q refers to the totally symmetric vibration belonging to a_{1g}. However, in second-order perturbations H_{vib} can couple $\Psi_g(r)$ with excited states, $\Psi_n(r)$, belonging to Γ_n, giving rise to a *decrement*, ΔE_g, of the ground-state energy

https://doi.org/10.1021/acs.inorgchem.4c00599
Inorg. Chem. 2024, 63, 13231−13243

$$\Delta E_g = -Q^2 \sum_n \frac{\langle \Psi_g(r)|V(r)|\Psi_n(r)\rangle^2}{E_n - E_g} \quad (3)$$

Thus, the excited states verifying $\Gamma_g \times \Gamma_n \supset \Gamma$ can be coupled to the ground state. This fact *modifies* the electronic density and also yields a *negative* contribution, $-K_\nu$,to the total force constant, K, which can be written as

$$K = K_0 - K_\nu \quad (4)$$

Here, K_0 stands for the positive contribution associated with the frozen electronic density of H_0 while K_ν reflects the electronic density changes due to H_{vib} and is given by

$$K_\nu = 2 \sum_n \frac{\langle \Psi_g(r)|V(r)|\Psi_n(r)\rangle^2}{E_n - E_g} \quad (5)$$

Thus, the instability responsible for the equilibrium structure of $CsMnF_4$ appears because the $K_0 < K_\nu$ condition is fulfilled in this case. Interestingly, this implies the admixture of the $^5A_{1g}$ ground state of MnF_6^{3-} with the excited $^5B_{1g}$ through a b_{1g} local mode, thus modifying the electronic density of the complex. It is worth noting that, in $CsMnF_4$, two adjacent MnF_6^{3-} units share a common ligand, a fact that is behind the instability developed in K_2CuF_4 or Cs_2AgF_4[23,9] but not in K_2ZnF_4:Cu^{2+}[23,9,60,61] or even in $KAlCuF_6$[68−70] where the CuF_6^{4-} units are well-separated. In addition, the parent phase of $CsMnF_4$ involves compressed MnF_6^{3-} units giving rise to softer bonds in the layer plane, a fact that also helps to develop the orthorhombic instability such as has previously been discussed.[23,9,22]

In the equilibrium geometry of $CsMnF_4$ at zero pressure the highest occupied molecular orbital (HOMO) wave function of the MnF_6^{3-} unit, $|\varphi_H\rangle$, is not purely $|x^2-y^2\rangle$ but involves an admixture of $|3z^2-r^2\rangle$ as a result of the symmetry reduction due to the instability

$$|\phi_H\rangle = \alpha|x^2 - y^2\rangle + \beta|3z^2 - r^2\rangle \quad (6)$$

The present calculations yield α^2 = 85%, stressing that the HOMO wave function keeps a dominant $|x^2-y^2\rangle$ character once the distortion takes place and $R_Y > R_X$. A similar situation has been found in other layered systems like K_2CuF_4 or Cs_2AgF_4.[23,9] Interestingly, if we write eq 6 using the $\{|x^2-z^2\rangle, |3y^2-r^2\rangle\}$ basis, then

$$|\phi_H\rangle = \alpha'|x^2 - z^2\rangle + \beta'|3y^2 - r^2\rangle \quad (7)$$

If α^2 = 85%, it is simple to find β'^2 = 98% demonstrating that the HOMO wave function is essentially $|3y^2-r^2\rangle$ and thus greatly localized along the longest Y axis. In the same way, the LUMO wave function, $|\varphi_L\rangle$, is basically equal to $|x^2-z^2\rangle$ despite the electronic structure of $CsMnF_4$ not being due to the JT effect.

For the sake of completeness, a qualitative picture of the electronic ground state of MnF_6^{3-} at the equilibrium geometry of $CsMnF_4$ at zero pressure is shown on Figure 3. Accordingly, the lowest d−d excitation is simply described by $|3y^2-r^2\rangle \rightarrow |x^2-z^2\rangle$. This matter will be discussed later.

Structural Changes Induced by Pressure. Results of calculations on $CsMnF_4$ under applied pressure were performed using both CRYSTAL and VASP codes. By means of them, we can derive the enthalpy per molecule, H = U + PV, responsible for the equilibrium structure at T = 0 K. Below P = 40 GPa the equilibrium structure of $CsMnF_4$ is always found to be described by the space group at ambient pressure ($P4/n$). The variations of lattice parameters and Mn−F distances induced by applied pressure are displayed in Table 3. Both codes lead to very similar results.

Table 3. Evolution of Lattice Parameters and Mn−F Distances for $CsMnF_4$ with Pressure Calculated with VASP (First Row) and CRYSTAL (Second Row) Codes[a]

P (GPa)	Symmetry	a (Å)	c (Å)	R_Z (Å)	R_X (Å)	R_Y (Å)
0	$P4/n$	8.029	6.401	1.829	1.871	2.189
		7.961	6.347	1.818	1.877	2.161
10	$P4/n$	7.649	5.970	1.802	1.858	2.058
		7.632	5.949	1.794	1.868	2.042
20	$P4/n$	7.442	5.763	1.784	1.839	1.997
		7.437	5.759	1.779	1.852	1.985
30	$P4/n$	7.282	5.632	1.771	1.821	1.957
		7.285	5.637	1.766	1.835	1.947
40	$P4/n$	7.146	5.545	1.760	1.806	1.925
		7.154	5.557	1.757	1.819	1.918
40	$P4$	7.172	5.430	1.755	1.833	1.939
		7.181	5.444	1.751	1.844	1.924
50	$P4$	6.988	5.532	1.745	1.853	1.851
		7.106	5.283	1.733	1.869	1.885

[a]Below P = 40 GPa the equilibrium structure is that observed at ambient pressure (space group $P4/n$) with MnF_6^{3-} units in the high-spin configuration (S = 2). At P = 40 GPa the $P4/n$ structure becomes unstable giving rise to a new equilibrium structure described by the $P4$ space group.

Nevertheless, at P = 40 GPa the present calculations indicate that the $P4/n$ structure becomes unstable, being slightly distorted to another one with a $P4$ space group (Figure 6). In both phases, the ground state of MnF_6^{3-} units is found to correspond to the high-spin configuration involving S = 2.

It should be noted that in the $P4$ phase at P = 40 GPa the MnF_6^{3-} complexes have local triclinic symmetry (point group C_1), with small distortions in the Mn−F distances and in the F−Mn−F angles with respect to the $P4/n$ structure at the same

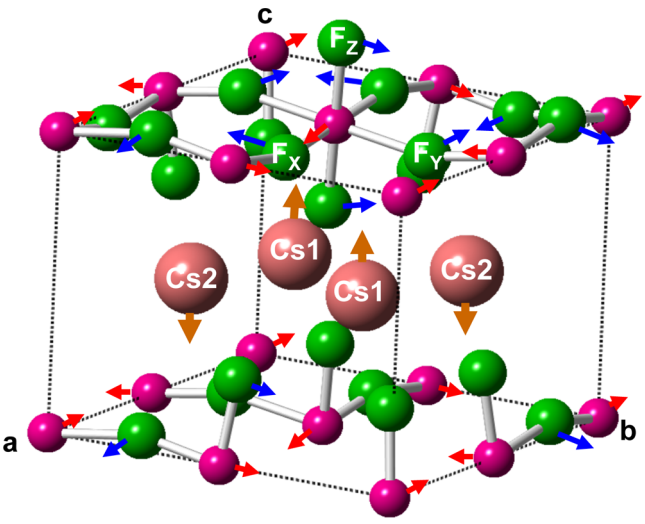

Figure 6. Qualitative picture of the small distortions produced by the unstable a_{2g} modes on the $P4/n$ structure of $CsMnF_4$ at P = 37.5 GPa producing the $P4$ phase, where the MnF_6^{3-} units have triclinic C_1 symmetry.

https://doi.org/10.1021/acs.inorgchem.4c00599
Inorg. Chem. 2024, 63, 13231−13243

pressure (see Figure S1 of the Supporting Information). For simplicity, Tables 3 and 5 show the average values of the Mn−F distances in the 3 local directions X, Y, and Z of the complexes, although the calculations of the d−d transitions have been carried out with the optimized geometries.

It should be also noted that within the $P4/n$ phase, the length reduction due to pressure is much bigger for the long bond of MnF_6^{3-} than for the two others. For instance, in the range 0−40 GPa, R_Y decreases by 0.25 Å while R_X and R_Z are reduced only by 0.03 and 0.07 Å, respectively (Table 3). In other words, pressure helps the geometry of the MnF_6^{3-} complex to become closer to the octahedral one as $R_Y - R_Z$ goes from 0.36 Å at ambient pressure to only 0.16 Å when P = 40 GPa. This behavior is very similar to that found for the hybrid layered perovskite $(C_2H_5NH_3)_2CdCl_4$ doped with Cu^{2+} and plays a key role for explaining the shifts undergone by d−d transitions under pressure,[71] a question analyzed in the next subsection.

Concerning the $P4/n \rightarrow P4$ phase transition at P = 40 GPa, calculations lead to an enthalpy difference $\Delta H = H(P4) - H(P4/n)$ equal only to −0.023 eV and −0.030 eV from VASP and CRYSTAL codes, respectively. It is worth noting that according to calculations, the three Mn−F distances of MnF_6^{3-} are only slightly influenced by the phase transition. Indeed, the variations undergone by R_X, R_Y, and R_Z at P = 40 GPa on changing from $P4/n$ to $P4$ are smaller than 1.4% (Table 3). This fact thus suggests that the $P4/n \rightarrow P4$ phase transition does not produce significant jumps in optical transitions, a matter treated in the next subsection.

Although the present calculations lead to an electronic ground state of MnF_6^{3-} units coming from the $^5E_g(t^3e^1)$ high-spin configuration in O_h symmetry, we have also paid attention to determine the enthalpy of the lowest state emerging from the $^3T_{1g}(t^4e^0)$ low-spin configuration in O_h symmetry. The difference of the enthalpy per molecule, ΔH, between low-sping (S = 1) and high-spin (S = 2) configurations derived for both the $P4/n$ and $P4$ structures at 40 and 50 GPa is displayed in Table 4. The calculated ΔH values by means of VASP and CRYSTAL codes are all in the range 0.45−0.68 eV. Therefore, the assumption of a transition from S = 2 to S = 1 induced by pressure at about 40 GPa[17] is highly unlikely.

Table 4. Difference of the Enthalpy Per Molecule, ΔH (in eV), between Low-Spin (S = 1) and High-Spin (S = 2) Configurations Calculated for Both $P4/n$ and $P4$ Phases at Pressures of P = 40 and 50 GPa[a]

P	Phase	ΔH
40	$P4/n$	0.63
		0.53
40	$P4$	0.65
		0.56
50	$P4/n$	0.48
		0.39
50	$P4$	0.45
		0.50

[a]Results obtained using VASP (first line) and CRYSTAL (second line) codes are both displayed.

Spin-Allowed d−d Transitions in $CsMnF_4$ under Pressure. Considering the equilibrium geometries derived for $CsMnF_4$ at different pressures in Table 3, we have calculated in a further step the evolution of spin-allowed d−d transitions for pressures up to 40 GPa using both VASP and CRYSTAL codes. Results displayed in Table 5 correspond to the $P4$ phase for P = 40 GPa and to the $P4/n$ phase for the rest of the pressures. Both codes lead to similar results.

Table 5. Calculated Energies (in eV) of Four Spin-Allowed d−d Transitions of MnF_6^{3-} Units in $CsMnF_4$ for Different Pressures, P (in GPa)[a]

P	Symmetry	$xy \rightarrow x^2-z^2$	$yz \rightarrow x^2-z^2$	$xz \rightarrow x^2-z^2$	$3y^2-r^2 \rightarrow x^2-z^2$
0	$P4/n$	2.83	2.48	2.18	1.84
		2.81	2.60	2.26	1.92
10	$P4/n$	2.94	2.53	2.33	1.55
		2.84	2.48	2.28	1.54
20	$P4/n$	3.02	2.63	2.45	1.44
		2.93	2.54	2.38	1.48
30	$P4/n$	3.10	2.73	2.57	1.38
			2.61	2.47	1.43
40	$P4$	2.99	2.72	2.56	1.47
		3.02	2.56	2.47	1.43

[a]First and second lines show the results obtained through VASP and CRYSTAL + ADF codes, respectively. The energies of all transitions are in eV. Note that data for P = 40 GPa correspond to the stable $P4$ phase, while for lower pressures the equilibrium structure corresponds to $P4/n$. Transitions are described though the dominant character of the involved orbitals. The influence of the internal electric field, $E_R(\mathbf{r})$, on the calculated d−d transitions is systematically taken into account.

The results presented in Table 5 show the existence of four allowed d−d transitions, in accord with the orthorhombic symmetry of MnF_6^{3-} units. As expected from Figure 3 the lowest d−d excitation actually corresponds to $|3y^2-r^2\rangle \rightarrow |x^2-z^2\rangle$ for all pressures.

The experimental spectrum of $CsMnF_4$ obtained at room temperature and ambient pressure (Figure 2) was assumed to involve only three spin-allowed d−d transition with energies[17] E_0 = 1.80 eV, E_1 = 2.26 eV, and $E_2 = E_3$ = 2.80 eV. According to Table 5, such transitions can now reasonably be assigned as $|3y^2-r^2\rangle \rightarrow |x^2-z^2\rangle$, $|xz\rangle \rightarrow |x^2-z^2\rangle$, and $|xy\rangle \rightarrow |x^2-z^2\rangle$, respectively. In the poorly resolved experimental spectrum (Figure 2), the $|yz\rangle \rightarrow |x^2-z^2\rangle$ transition, calculated at about 2.55 eV, is not well seen likely due to the width of the $|xz\rangle \rightarrow |x^2-z^2\rangle$ and $|xy\rangle \rightarrow |x^2-z^2\rangle$ transitions as well as to the presence of spin-forbidden transitions in the spectrum.

The calculated evolution of four spin-allowed d−d transitions with pressure (Table 5) is depicted in Figure 7. It should be noted that the first $|3y^2-r^2\rangle \rightarrow |x^2-z^2\rangle$ transition experiences a drastic red shift with pressure as it moves from 1.84 eV at zero pressure to 1.47 eV at P = 40 GPa. By contrast, the three transitions associated with t_{2g} orbitals in O_h symmetry undergo a moderate blue-shift under pressure. Interestingly, the energy difference, $\Delta(xy,xz)$, between $|xy\rangle \rightarrow |x^2-z^2\rangle$ and $|xz\rangle \rightarrow |x^2-z^2\rangle$ transitions is reduced significantly on passing from zero ($\Delta(xy,xz)$ = 0.65 eV) to 40 GPa ($\Delta(xy,xz)$ = 0.43 eV). At the same time, the energies of the two transitions associated with $|xz\rangle$ and $|yz\rangle$ orbitals become equal within ∼0.1 eV at P = 40 GPa such as it is shown in Table 5. Therefore, the very broad band observed at around 40 GPa that peaked at 2.5 eV likely involves the unresolved contributions of three transitions associated with the three t_{2g} orbitals in O_h symmetry.

The evolution of four spin-allowed d−d transitions of $CsMnF_4$ under pressure (Table 5 and Figure 7) is consistent

https://doi.org/10.1021/acs.inorgchem.4c00599
Inorg. Chem. 2024, 63, 13231−13243

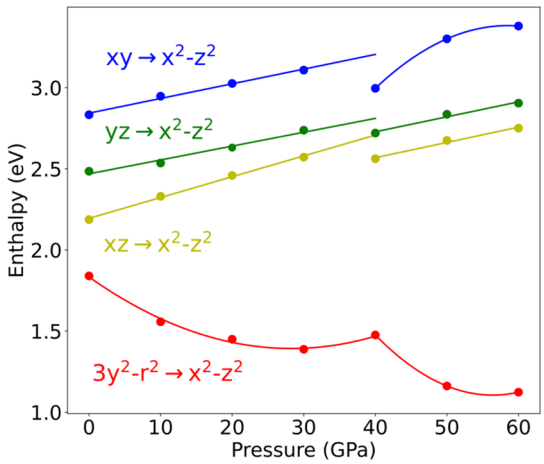

Figure 7. Variation of the four d−d transition energies of $CsMnF_4$ in the 0−60 GPa pressure range. Values were calculated with the VASP code, but similar variations were obtained with CRYSTAL + ADF codes.

with the calculated variations undergone by the Mn−F distances (Table 3). Indeed, we have seen that pressure favors a geometry of the MnF_6^{3-} complex progressively closer to the octahedral one thus reducing $\Delta(xy,xz)$ as well as the energy of the $|3y^2-r^2\rangle \rightarrow |x^2-z^2\rangle$ transition. Along this line, we have found that R_Y related to the softest Mn−F bond is much more reduced by pressure than R_X or R_Z (Table 3), and thus, we can reasonably expect a red-shift for that transition under pressure. This behavior is fully similar to that found in hybrid layered perovskites[69] like $(CH_3NH_3)_2CuCl_4$, $(C_2H_5NH_3)_2CuCl_4$, or $(C_2H_5NH_3)_2CdCl_4$:Cu^{2+}.

In a further step, it is necessary to disclose the influence of the internal field $E_R(r)$ on the optical transitions of $CsMnF_4$ as it plays an important role in the case of inorganic layered perovskites like K_2CuF_4 or Cs_2AgF_4.[6,8,23] For clarifying this issue, we have calculated in a first step the energies of four d−d transitions considering only the *isolated* MnF_6^{3-} unit at the equilibrium geometry while in a second step we have added the influence of the electrostatic potential, $V_R(\mathbf{r})$. Results have been derived for P = 0 and 20 GPa and are shown in Table 6. It can be noticed that the addition of $\mathbf{E}_R(\mathbf{r})$ produces an important shift of about 0.5 eV on the energy of the lowest d−d transition, a result qualitatively consistent with the shape of $V_R(\mathbf{r})$ (Figure 4). Indeed $(-e)V_R(\mathbf{r})$ tends to decrease the energy of orbitals, such as $|3y^2-r^2\rangle$, lying in the layer plane thus enhancing the $|3y^2-r^2\rangle \rightarrow |x^2-z^2\rangle$ transition energy. A similar situation is encountered in K_2CuF_4 or Cs_2AgF_4.[23]

Finally, for the sake of clarity, we have performed an analysis of three contributions responsible for the energy E_0 of the first spin-allowed transition $|3y^2-r^2\rangle \rightarrow |x^2-z^2\rangle$ of $CsMnF_4$ at zero pressure. According to the present discussion, we divide the calculation in 3 steps: (1) We consider an isolated MnF_6^{3-} unit in the tetragonal geometry of the parent phase, obtaining a value E_0 = 0.89 eV. (2) In a second step, we still keep the isolated MnF_6^{3-} unit but in the final $P4/n$ geometry where MnF_6^{3-} exhibits a practical orthorhombic symmetry with $R_Y - R_X$ = 0.31 Å, obtaining E_0 = 1.44 eV. (3) In the final step, we include the shift due to the internal $V_R(\mathbf{r})$ potential on the energy of the transition, obtaining a value E_0 = 1.92 eV. Therefore, the contributions of both the orthorhombic distortion and $V_R(\mathbf{r})$ enhance the E_0 value by ∼1 eV.

Survey of Other Compounds Containing MnF_6^{3-} Units. Thanks to the analysis carried out in preceding sections on $CsMnF_4$ we can now gain better insight into the different optical properties at zero pressure displayed by other fluorides involving Mn^{3+}. In a first step we pay attention to the Na_3MnF_6 compound[12,13] where the metal−ligand distances are R_z = 2.018 Å, R_x = 1.862 Å, and R_y = 1.897 Å. Accordingly, in this case the longest metal−ligand distance is along the Z axis, the orthorhombicity is small ($R_y - R_x$ = 0.035 Å), and the HOMO practically equal to $|3z^2-r^2\rangle$. The energies of allowed d−d transitions measured experimentally[12] and derived by means of first-principles calculations[13] are reported in Table 7. It can be seen that the transitions $|t_i\rangle \rightarrow |3z^2-r^2\rangle$ (t = *xy*, *xz*, *yz*) all are in the 2−3 eV range, as has been found for $CsMnF_4$. However, the energy of the first $|3z^2-r^2\rangle \rightarrow |x^2-y^2\rangle$ transition is practically half the value E_0 = 1.9 eV obtained for $CsMnF_4$, thus involving a remarkable difference. A similar situation is encountered when looking at the first transition of K_3MnF_6 or Cs_3MnF_6 where E_0 = 1.1 eV.[72,57]

There are two main reasons behind a E_0 value around 1 eV for Na_3MnF_6. On one hand, the orthorhombicity of MnF_6^{3-} units in this compound is 1 order of magnitude smaller than that found for $CsMnF_4$. On the other hand, Na_3MnF_6 is not a typical layered compound like K_2CuF_4 or $CsMnF_4$ and the internal electric field, $\mathbf{E}_R(\mathbf{r})$, has proven to induce shifts on d−d transitions not higher than 0.1 eV.[13]

It is worth noting now that a similar situation has been found when comparing fluoride compounds containing Cu^{2+}, such as $KZnF_3$:Cu^{2+}, K_2ZnF_4:Cu^{2+}, and K_2CuF_4. As $KZnF_3$ is cubic there is a static JT effect in $KZnF_3$:Cu^{2+}, with an unpaired electron in $|x^2-y^2\rangle$.[73−75] Due to the cubic symmetry

Table 6. Influence of the Internal Electric Field, $\mathbf{E}_R(\mathbf{r})$, on the Energy (in eV) of Four d−d Transitions Corresponding to MnF_6^{3-} Units in $CsMnF_4$ for Two Pressures, P = 0 and 20 GPa[a]

Pressure	$xy \rightarrow x^2-z^2$	$yz \rightarrow x^2-z^2$	$xz \rightarrow x^2-z^2$	$3y^2-r^2 \rightarrow x^2-z^2$
0	2.62	2.51	2.23	1.44
	2.81	2.60	2.26	1.92
20	2.69	2.54	2.38	0.95
	2.93	2.54	2.38	1.48

[a]The first row corresponds to calculated values with CRYSTAL + ADF codes on an isolated MnF_6^{3-} unit at the equilibrium geometry corresponding to the applied pressure, while in the second row are shown the values derived including the electrostatic potential $V_R(\mathbf{r})$ in the calculation. Transitions are described though the dominant character of involved orbitals.

Table 7. Energies of Spin-Allowed d−d Transitions for MnF_6^{3-} Units in Na_3MnF_6 Derived at Ambient Pressure[a]

	$3z^2-r^2 \rightarrow x^2-y^2$	$xy \rightarrow x^2-y^2$	$xz \rightarrow x^2-y^2$	$yz \rightarrow x^2-y^2$	ref.
Experimental	1.04	2.18	2.38	2.38	54
		2.17	2.38	2.58	12
Calculated	0.71	2.11	2.27	2.32	13

[a]In this compound the metal−ligand distances[12] are R_z = 2.018 Å, R_x = 1.862 Å, and R_y = 1.897 Å giving rise to a small orthorhombicity ($R_y - R_x$ = 0.035 Å) and a HOMO practically equal to $|3z^2-r^2\rangle$. Transition energies (in eV) have been obtained from both experiments and calculations.

https://doi.org/10.1021/acs.inorgchem.4c00599
Inorg. Chem. 2024, 63, 13231−13243

of the host lattice, $\mathbf{E}_R(\mathbf{r})$ has no effect on the first d−d transition, $|3z^2-r^2\rangle \rightarrow |x^2-y^2\rangle$, whose energy is E_0 = 0.40 eV.[74,75] As K_2ZnF_4 is a layered compound where the shape of $V_R(\mathbf{r})$ is similar to that of Figure 4, the unpaired electron is forced to be in a $|3z^2-r^2\rangle$ orbital by the action of $V_R(\mathbf{r})$, and consequently the $|x^2-y^2\rangle \rightarrow |3z^2-r^2\rangle$ transition energy is enhanced having a value E_0 = 0.70 eV.[76,61,74] Finally, as in K_2CuF_4 two adjacent CuF_6^{4-} units share a common ligand, this favors an orthorhombic instability which still increases the E_0 value up to 1.03 eV.[77,78,74,9]

Magnetic Structure of $CsMnF_4$: Influence of Pressure. As shown in Figure 8, the present calculations support that in

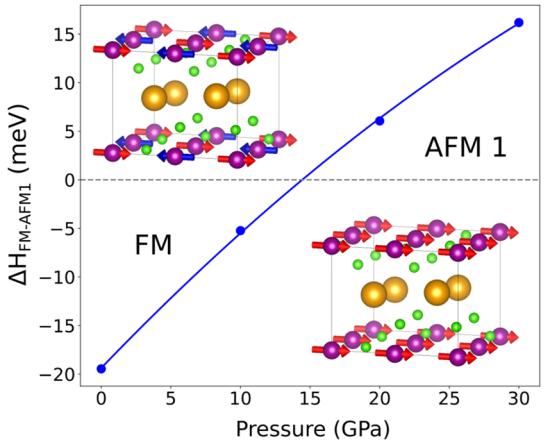

Figure 8. Evolution of magnetic ordering in $CsMnF_4$ as a function of pressure. In the figure is depicted the enthalpy difference (given per formula unit, in meV) between ferromagnetic and antiferromagnetic ordering calculated for pressures up to 30 GPa where $CsMnF_4$ is always in the $P4/n$ structure.

$CsMnF_4$ at ambient pressure layers are ferromagnetically ordered. This behavior, consistent with experimental data, is the same found for layered compounds like K_2CuF_4 or Cs_2AgF_4 where the M−F−M angle, θ, (M = Cu, Ag) is 180° due to the absence of buckling at the *Cmca* equilibrium structure.[9,22] The ferromagnetism displayed by K_2CuF_4 or Cs_2AgF_4 is surprising as tetragonal K_2MnF_4 and K_2NiF_4 compounds, where the θ angle is also equal to 180°, exhibit an AFM ordering the same found for $KMnF_3$ and $KNiF_3$ perovskites.[79] Very recently, the ferromagnetism in K_2CuF_4 and Cs_2AgF_4 at the *Cmca* equilibrium structure has proved to come from the orthorhombic distortion undergone by MF_6^{4-} units (M = Cu, Ag), which in turn is actually responsible for the orbital ordering in these compounds.[22] Indeed, in the *I*4/*mmm* parent phase of K_2CuF_4 and Cs_2AgF_4, involving tetragonal MF_6^{4-} units (M = Cu, Ag), the calculations lead to an AFM ordering similar to that observed for K_2MnF_4 or K_2NiF_4 at ambient pressure.

We verified that a similar situation holds for $CsMnF_4$. Indeed, in the *P*4/*nmm* parent phase, where $R_y = R_x$ we also find that the layers of $CsMnF_4$ are AFM ordered although the FM ordering has an energy that is only 20.6 meV above (Figure 9). Moreover, on passing progressively at zero pressure from the *P*4/*nmm* parent phase to the equilibrium *P*4/*n* structure, $CsMnF_4$ easily becomes ferromagnetic following the increase of the orthorhombic distortion on the MnF_6^{3-} units, as shown in Figure 9.

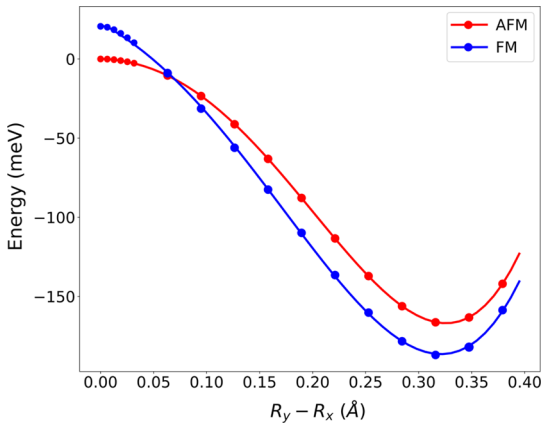

Figure 9. Energy (given per formula unit) of $CsMnF_4$ obtained by single-point calculations throughout the antiferrodistortive distortion from the parent tetragonal *P*4/*nmm* phase ($R_Y - R_X = 0$) to the *P*4/*n* structure where $R_Y - R_X$ = 0.32 Å at equilibrium. In this process, the AFM and FM ordering in the layers of $CsMnF_4$ are both considered.

It is worth noting that, on passing from $R_Y - R_X = 0$ to $R_Y - R_X$ = 0.32 Å, the orthorhombic distortion implies an energy gain of 206.7 and 166.7 meV for the FM and AFM ordering, respectively (Figure 9). These values are thus 1 order of magnitude higher than the energy difference (20.6 meV) between both magnetic structures at the *P*4/*nmm* parent phase. This simple result just stresses that vibronic interactions, which are behind the orthorhombic MnF_6^{3-} units at equilibrium, play an important role for explaining the magnetic structure in $CsMnF_4$.

In K_2CuF_4 and Cs_2AgF_4, the shift from AFM to FM ordering when $R_y - R_x$ increases has proved to arise from deep changes in chemical bonding in the MF_6^{4-} units (M = Cu, Ag). Indeed, an increase of the orthorhombicity enhances the charge, $q(R_X)$, transferred to the closest ligands, placed at R_X from the cation, at the expense of two ligands at R_Y whose charge, $q(R_Y)$, is drastically reduced, being null at equilibrium.[22] As the AFM contribution to the exchange constant depends on $q(R_X) \times q(R_Y)$, this fact favors the shift to a FM phase.[22]

When pressure increases, the results of the present calculations (Figure 8) reveal that above a pressure of 15 GPa the layers of $CsMnF_4$ should be AFM ordered. Experimental data with pressures up to 4 GPa obtained by Ishizuka et al.[80] show that the critical temperature, T_c, decreases with pressure, a fact qualitatively consistent with results gathered in Figure 8. Along this line, recent GGA+U calculations by Behatha et al.[81] also find a transition from the ferromagnetic to the AFM ordering although at a lower pressure of 2.4 GPa.

Two relevant facts are behind the pressure-induced shift from FM to AFM ordering in $CsMnF_4$ shown in Figure 8. On one hand, there is a significant reduction of the orthorhombicity (Table 3). Indeed, while $R_y - R_x$ = 0.32 Å at zero pressure, it becomes 44% smaller under a pressure of 15 GPa. On the other hand, the Mn−F−Mn angle in $CsMnF_4$ changes from θ = 162.6° at zero pressure to θ = 153.4° at P = 15 GPa. Although in this process θ changes only by 5.7%, we have to recall that $RbMnF_4$ at zero pressure (space group $P2_1/a$) is AFM with a very low transition temperature (4 K) and an angle θ equal to 148°.[19]

https://doi.org/10.1021/acs.inorgchem.4c00599
Inorg. Chem. 2024, 63, 13231−13243

CONCLUSIONS

The existence of an orthorhombic instability plays a central role in understanding the optical and magnetic properties of layered compounds like $CsMnF_4$ or K_2CuF_4. However, that instability is surprisingly not developed in $CsFeF_4$ whose structure belongs to the *P*4/*nmm* space group and the FeF_6^{3-} units are essentially tetragonal with $R_x = R_y$.

According to eq 3, a negative force constant requires the admixture of the electronic ground state, $\Psi_g(r)$, with an excited state, $\Psi_n(r)$, via operator $V(\mathbf{r})$ reflecting the electron−vibration coupling. As $V(\mathbf{r})$ is a purely orbital operator, a necessary condition for having such an admixture and a force constant $K < 0$ is a matrix element $\langle \Psi_g(\mathbf{r}), S_g | V(\mathbf{r}) | \Psi_n(\mathbf{r}), S_n \rangle$ different from zero, where S_g and S_n stand for the spin of ground and excited states, respectively. As FeF_6^{3-} complexes in $CsFeF_4$ are in a high-spin configuration this means a ground state with $S_g = 5/2$. If we now consider all excited states emerging from the d^5 configuration of free Fe^{3+} ion, there are a total of 246 states.[43] However, in such excited states the spin is at most $S_n = 3/2$ and thus none of them can be coupled to the $^6A_{1g}$ state of the FeF_6^{3-} unit. This spin barrier thus hampers the existence of orthorhombic instability in high-spin complexes of Fe^{3+} or Mn^{2+} ions.

That barrier does not exist for MnF_6^{3-} complexes in $CsMnF_4$ as the $^5A_{1g}$ ground state can be mixed with excited $^5B_{1g}$ through the orthorhombic b_{1g} mode. A similar situation holds for CuF_6^{4-} units in layered lattices like K_2CuF_4, where the orthorhombic distortion has been shown to be directly responsible for its surprising FM behavior.[9,22]

By contrast, for tetragonal CrF_6^{3-} complexes, there is also a hindrance against orthorhombic instability. Under O_h symmetry the ground state of CrF_6^{3-} is $^4A_{2g}$ which becomes $^4B_{1g}$ in D_{4h}. Among the 120 multiplets arising from the d^3 configuration of free Cr^{3+} ion, only the states $^4T_{1g}$ and $^4T_{2g}$ have the same spin $S = 3/2$ as the ground state $^4A_{2g}$ in O_h symmetry.[43] Thus, a $^4B_{1g}$ ground state in D_{4h} symmetry requires $^4A_{1g}$ excited states for having a nonzero vibronic coupling associated with the b_{1g} mode. However, neither $^4T_{1g}$ nor $^4T_{2g}$ give rise to $^4A_{1g}$ states under the $O_h \rightarrow D_{4h}$ symmetry reduction. No orthorhombic distortion is observed for the tetragonal K_2MgF_4 compound doped with Cr^{3+}.[82,83] A similar lack of excited states for tetragonal NiF_6^{4-} units hampers the orthorhombic instability in K_2NiF_4.[22]

These reasons thus underline the origin of low-symmetry complexes widely observed for Cu^{2+} or Mn^{3+} systems and are not due to the Jahn−Teller effect. They are also behind the so-called plasticity property of compounds of Cu^{2+} and Mn^{3+} ions.[84]

We have seen that in $CsMnF_4$ the internal electric field, $\mathbf{E}_R(\mathbf{r})$, *increases* the value of the first d−d excitation by 0.5 eV, and a similar effect takes place in other layered compounds like K_2CuF_4.[23] It is worth noting now that this behavior is not necessarily general, as in other systems $\mathbf{E}_R(\mathbf{r})$ can give rise to an energy *reduction*. This is just what happens in the singular compound $CaCuSi_4O_{10}$, the basis for the historical Egyptian blue pigment,[85] involving square-planar CuO_4^{6-} complexes. In that compound the internal electric field produces a reduction of 0.9 eV in the highest d−d transition, which is thus directly responsible for its blue color.[86]

According to the present discussion, the behavior of d^4 and d^9 ions in tetragonal insulating lattices can hardly be ascribed to the Jahn−Teller effect. Along this line it is worth noting that even when such ions are initially located in a cubic symmetry there is not necessarily a static Jahn−Teller effect.[87] For instance, in the Cu^{2+}-doped cubic $SrCl_2$ compound, the Cu^{2+} ion, initially replacing Sr^{2+}, experiences a big off-center motion along ⟨001⟩ type directions driven by a force constant that becomes negative.[88,89] A similar situation is found for Ag^{2+} and Ni^+ in $SrCl_2$ and also for SrF_2:Cu^{2+} and CaF_2:Ni^+.[87]

Further work on the optical and magnetic properties of insulating transition metal compounds is now underway.

ASSOCIATED CONTENT

Supporting Information

The Supporting Information is available free of charge at https://pubs.acs.org/doi/10.1021/acs.inorgchem.4c00599.

Additional computational details for both CRYSTAL17 (S1)25-27, and VASP codes (S2) and equilibrium geometries (S3); equilibrium geometries for *P*4/*n* phase at $P = 0$ GPa for $S = 2$, *P*4/*n* phase at $P = 40$ GPa for $S = 2$, and *P*4 phase at $P = 40$ GPa for $S = 2$ (PDF)

AUTHOR INFORMATION

Corresponding Author

Toraya Fernández-Ruiz − *Departamento de Ciencias de la Tierra y Física de la Materia Condensada, Universidad de Cantabria, 39005 Santander, Spain;* orcid.org/0000-0001-8597-7133; Email: fernandezrt@unican.es

Authors

Guillermo Santamaría − *Departamento de Ciencias de la Tierra y Física de la Materia Condensada, Universidad de Cantabria, 39005 Santander, Spain; Donostia International Physics Center (DIPC), 20018 Donostia, Euskadi, Spain; Laboratory for Chemistry of Novel Materials, University of Mons, 7000 Mons, Belgium*

Juan María García-Lastra − *Department of Energy Conversion and Storage, Technical University of Denmark, 2800 Kgs. Lyngby, Denmark;* orcid.org/0000-0001-5311-3656

Pablo García-Fernández − *Departamento de Ciencias de la Tierra y Física de la Materia Condensada, Universidad de Cantabria, 39005 Santander, Spain;* orcid.org/0000-0002-4901-0811

Inés Sánchez-Movellán − *Departamento de Ciencias de la Tierra y Física de la Materia Condensada, Universidad de Cantabria, 39005 Santander, Spain*

Miguel Moreno − *Departamento de Ciencias de la Tierra y Física de la Materia Condensada, Universidad de Cantabria, 39005 Santander, Spain*

José Antonio Aramburu − *Departamento de Ciencias de la Tierra y Física de la Materia Condensada, Universidad de Cantabria, 39005 Santander, Spain;* orcid.org/0000-0002-5030-725X

Complete contact information is available at: https://pubs.acs.org/10.1021/acs.inorgchem.4c00599

Author Contributions

†G.S. and T.F.-R. contributed equally to this work.

Notes

The authors declare no competing financial interest.

https://doi.org/10.1021/acs.inorgchem.4c00599
Inorg. Chem. 2024, 63, 13231−13243

■ ACKNOWLEDGMENTS

The support by the Spanish Ministerio de Ciencia y Tecnología under Project PID2022-139776NB-C63 is acknowledged. T.F.-R. acknowledges financial support from Grant PRE2019-089054 funded by MCIN/AEI/10.13039/501100011033 and by ESF Investing in your future. G.S. acknowledges the financial support from Universidad de Cantabria and DIPC.

■ REFERENCES

(1) Moulton, P. F. Spectroscopic and laser characteristics of Ti:Al_2O_3. *J. Opt. Soc. America B* **1986**, *3*, 125−133.
(2) Powell, R. C. In *Physics of solid-state laser materials*; Springer: New York, 1998; pp 1−9, 215. DOI: 10.1007/978-1-4612-0643-9.
(3) Doroshenko, M. E.; Osiko, V. V.; Jelínková, H.; Jelínek, M.; Šulc, J.; Vyhlídal, D.; Kovalenko, N. O.; Terzin, I. S. Spectral and lasing characteristics of Fe:$Cd_{1-x}Mn_xTe$ (x = 0.1 - 0.76) crystals in the temperature range 77 to 300 K. *Opt. Mater. Express* **2018**, *8*, 1708−1722.
(4) Singh, R. J. Some Important Features of Manganites. *J. Mod. Phys.* **2013**, *4*, 191−199.
(5) Li, X.; Zhong, X.; Hu, Y.; Li, B.; Sheng, Y.; Zhang, Y.; Weng, C.; Feng, M.; Han, H.; Wang, J. Organic-Inorganic Copper(II)-Based Material: A Low-Toxic, Highly Stable Light Absorber for Photovoltaic Application. *J. Phys. Chem. Lett.* **2017**, *8*, 1804−1809.
(6) Garcia-Fernandez, P.; Moreno, M.; Aramburu, J. A. Electrostatic Control of Orbital Ordering in Noncubic Crystals. *J. Phys. Chem. C* **2014**, *118*, 7554−7561.
(7) Khomskii, D. I.; Streltsov, S. V. Orbital Effects in Solids: Basics, Recent Progress, and Opportunities. *Chem. Rev.* **2021**, *121*, 2992−3030.
(8) Bersuker, I. B. Pseudo Jahn-Teller Effect—A Two-State Paradigm in Formation, Deformation, and Transformation of Molecular Systems and Solids. *Chem. Rev.* **2013**, *113*, 1351−1390.
(9) Sánchez-Movellán, I.; Moreno, M.; Aramburu, J. A.; García-Fernández, P. Strain-Induced Ferromagnetic to Antiferromagnetic Crossover in d^9-Ion (Cu^{2+} and Ag^{2+})-Layered Perovskites. *J. Phys. Chem. C* **2023**, *127* (33), 8332−8341.
(10) Drickamer, H. G.; Frank, C. W. In *Electronic Transitions and the High Pressure Chemistry and Physics of Solids*; Chapman Hall: London, 1973; pp 72−109. ISBN: 978-0412116506.
(11) Reber, C.; Grey, J. K.; Lanthier, E.; Frantzen, K. A. Pressure-induced change of d-d Luminescence Energies, Vibronic Structure and Band Intensities in Transition. *Comm. Inorg. Chem.* **2005**, *26*, 233−254.
(12) Carlson, S.; Xu, Y.; Halenius, U.; Norrestam, R. A Reversible, Isosymmetric, High-Pressure Phase Transition in Na_3MnF_6. *Inorg. Chem.* **1998**, *37*, 1486−1492.
(13) Sánchez-Movellán, I.; Carrasco-Busturia, D.; García-Lastra, J. M.; García-Fernández, P.; Aramburu, J. A.; Moreno, M. Pressure Effects on $3d^n$ (n = 4, 9) Insulating Compounds: Long Axis Switch in Na_3MnF_6 not Due to the Jahn-Teller Effect. *Chem.—Eur. J.* **2022**, *28*, e202200948.
(14) Dolan, J. F.; Rinzler, A. G.; Kappers, L. A.; Bartram, R. H. Pressure and temperature dependence of chromium photoluminescence spectra in fluoride elpasolites. *J. Phys. Chem. Solids* **1992**, *53*, 905−912.
(15) Freire, P. T. C.; Pilla, O.; Lemos, V. Pressure-induced level crossing in $KZnF_3:Cr^{3+}$. *Phys. Rev. B* **1994**, *49*, 9232−9235.
(16) Ksenofontov, V.; Gaspar, A. B.; Gutlich, P. Pressure Effect Studies on Spin Crossover and Valence Tautomeric Systems. *Top. Curr. Chem.* **2004**, *235*, 23−64.
(17) Aguado, F.; Rodriguez, F.; Núñez, P. Pressure-induced Jahn-Teller suppression and simultaneous high-spin to low-spin transition in the layered perovskite $CsMnF_4$. *Phys. Rev. B* **2007**, *76*, 094417.
(18) Molinier, M.; Massa, W. Die Kristallstrukturen der Tetrafluoromanganate(III) $AMnF_4$ (A = K, Rb, Cs). *Z. Naturforsch.* **1992**, *47b*, 783−788.
(19) Molinier, M.; Frommen, Ch.; Massa, W.; Pebler, J.; Roisnel, Th. Magnetism of Alkalitetrafluoromanganates (III) $AMnF_4$ (A = K, Rb, Cs): Neutron Diffraction, Mössbauer and Magnetization Investigations. *Z. Naturforsch.* **1993**, *48a*, 1054−1072.
(20) Massa, W. Structural Chemistry and Jahn-Teller Effect in Fluoromanganates(III). *Rev. Inorg. Chem.* **1999**, *19*, 117−183.
(21) Moron, M. C.; Palacio, F.; Clark, S. M. Pressure-induced structural phase transitions in the $AMnF_4$ series (A = Cs, Rb, K) studied by synchrotron x-ray powder diffraction: Correlation between hydrostatic and chemical pressure. *Phys. Rev. B* **1996**, *54*, 7052−7061.
(22) Sanchez-Movellan, I.; Santamaria-Fernandez, G.; Garcia-Fernandez, P.; Aramburu, J. A.; Moreno, M. Understanding the Local Structure, Magnetism, and Optical Properties in Layered Compounds with d^9 Ions: Insight into Silver Fluorides and K_2CuF_4. *J. Phys. Chem. C* **2023**, *127*, 16695−16708.
(23) Aramburu, J. A.; García-Fernández, P.; Mathiesen, N. R.; García-Lastra, J. M.; Moreno, M. Changing the Usual Interpretation of the Structure and Ground State of Cu^{2+}-Layered Perovskites. *J. Phys. Chem. C* **2018**, *122*, 5071−5082.
(24) Dovesi, R. et al. CRYSTAL17 User's Manual (University of Torino, Torino), 2017.
(25) Peintinger, M. F.; Oliveira, D. V.; Bredow, T. J. Consistent Gaussian basis sets of triple-zeta valence with polarization quality for solid-state calculations. *J. Comput. Chem.* **2013**, *34*, 451−459.
(26) CRYSTAL basis sets. https://www.crystal.unito.it/basis_sets.html (accessed on May 29, 2022).
(27) Bredow, T.; Gerson, A. Effect of exchange and correlation on bulk properties of MgO, NiO, and CoO. *Phys. Rev. B* **2000**, *61*, 5194−5201.
(28) Kresse, G.; Hafner, J. *Ab initio* molecular-dynamics simulation of the liquid-metal-amorphous-semiconductor transition in germanium. *Phys. Rev. B* **1994**, *49*, 14251−14269.
(29) Kresse, G.; Furthmüller, J. Efficient iterative schemes for *ab initio* total-energy calculations using a plane-wave basis set. *Phys. Rev. B* **1996**, *54*, 11169−11186.
(30) Blöchl, P. E. Projector augmented-wave method. *Phys. Rev. B* **1994**, *50*, 17953−17979.
(31) Kresse, G.; Joubert, D. From ultrasoft pseudopotentials to the projector augmented-wave method. *Phys. Rev. B* **1999**, *59*, 1758−1775.
(32) Heyd, J.; Scuseria, G. E.; Ernzerhof, M. Hybrid functionals based on a screened Coulomb potential. *J. Chem. Phys.* **2003**, *118*, 8207−8215.
(33) Press, W. H.; Teukolsky, S. A.; Vetterling, W. T.; Flannery, B. P. *Numerical Recipes: The Art of Scientific Computing*; Cambridge University Press: New York, 1986.
(34) Shannon, R. D. Revised effective ionic radii and systematic studies of interatomic distances in halides and chalcogenides. *Acta Crystallogr.* **1976**, *A32*, 751−767.
(35) Hidaka, M.; Fujii, H.; Garrard, B. J.; Wanklyn, B. M. Structural phase transitions in the layer compound $CsFeF_4$. *Phys. St. Solidi A* **1986**, *95*, 413−421.
(36) te Velde, G.; Bickelhaupt, F. M.; Baerends, E. J.; Guerra, C. F.; van Gisbergen, S. J.; Snijders, J. D.; Ziegler, T. Chemistry with ADF. *J. Comput. Chem.* **2001**, *22*, 931−967.
(37) Becke, A. D. Density-functional thermochemistry. III. The role of exact exchange. *J. Chem. Phys.* **1993**, *98*, 5648−5652.
(38) Moreno, M.; Aramburu, J. A.; Barriuso, M. T. Electronic Properties and Bonding in Transition Metal Complexes: Influence of Pressure. In *Optical Spectra and Chemical Bonding in Inorganic Compounds*; Mingos, D. M. P., Schönherr, T., Eds.; Structure and Bonding, vol. *106*; Springer: Berlin, 2004; pp 127−152. DOI: 10.1007/b11309.
(39) Van Gool, W.; Piken, A. G. Lattice self-potentials and Madelung constants for some compounds. *J. Mater. Sci.* **1969**, *4*, 95−104.
(40) Tosi, M. P. Cohesion of Ionic Solids in the Born Model. *Solid State Phys.* **1964**, *16*, 1−120.

(41) Gorling, A. Density-functional theory beyond the Hohenberg-Kohn theorem. *Phys. Rev. A* **1999**, *59* (5), 3359−3374.
(42) Hellman, A.; Razaznejad, B.; Lundqvist, B. I. Potential-energy surfaces for excited states in extended systems. *J. Chem. Phys.* **2004**, *120* (10), 4593−4602.
(43) Sugano, S.; Tanabe, Y.; Kamimura, H. *Multiplets of transition metal ions in crystals*; Academic Press: New York, 1970; pp 263−270
(44) Abragam, A.; Bleaney, B. *Electron Paramagnetic Resonance of Transition Ions*; Clarendon Press: Oxford, 1970; pp 461. ISBN: 978-0-19-965152-8.
(45) Reinen, D.; Friebel, C.; Propach, V. High- und Low-Spin-Verhalten des Ni^{3+} -Ions in oktaedrischer Koordination. (A) NiF_6^{3-},-Polyeder. *Z. anorg. allg. Chem.* **1974**, *408*, 187−204.
(46) Reinen, D.; Atanasov, M.; Köhler, P.; Babel, D. Jahn-Teller coupling and the influence of strain in Tg and Eg ground and excited states - A ligand field and DFT study on halide $M^{III}X_6$ model complexes [M = Ti^{III}-Cu^{III};X = F^-, Cl^-]. *Coord. Chem. Rev.* **2010**, *254*, 2703−2754.
(47) Aramburu, J. A.; García-Fernández, P.; García-Lastra, J. M.; Moreno, M. A genuine Jahn-Teller system with compressed geometry and quantum effects originating from zero-point motion. *ChemPhysChem* **2016**, *17*, 2146−2156.
(48) Hall, T. P. P.; Hayes, W.; Stevenson, R. W. H.; Wilkens, J. Investigation of the bonding of iron-group ions in fluoride crystal. II. *J. Chem. Phys.* **1963**, *39*, 35−39.
(49) Alcalá, R.; Villacampa, B. EPR study of Ni3+ centers in $CsCaF_3$. *Solid State Commun.* **1994**, *90*, 13−16.
(50) Grannec, J.; Lozano, L.; Sobre, P.; Portier, J.; Hagenmuller, P. Sur un nouvel hexafluorure de nickel trivalent de formule Li_3NiF_6. *J. Fluor. Chem.* **1975**, *6*, 267−274.
(51) Lim, P. E.; Stout, J. W. Polarized crystal spectra of CrF_2 from 6000 to 38 OOO cm^{-1}. *J. Chem. Phys.* **1975**, *63*, 4886−4902.
(52) Duclos, S. J.; Vohra, Y. K.; Ruoff, A. L. Pressure dependence of the $^4T_2$ and $^4T_1$ absorption bands of ruby to 35 GPa. *Phys. Rev. B* **1990**, *41* (8), 5372−5381.
(53) García-Lastra, J. M.; García-Fernandez, P.; Barriuso, M. T.; Aramburu, J. A.; Moreno, M. Sharp Lines Due to Cr^{3+} and Mn^{2+} Impurities in Insulators: Going Beyond the Usual Tanabe-Sugano Approach. *J. Phys. Chem. A* **2014**, *118*, 2377−2384.
(54) Ham, F. S. Jahn-Teller effects in *Electron Paramagnetic Resonance spectra. In Electron Paramagnetic Resonance*; Geschwind, S., Ed.; Plenum: New York, 1972; pp 1−119.
(55) Bill, H. *Observation of the Jahn-Teller Effect with Electron Paramagnetic Resonance in The Dynamical Jahn-Teller Effect in Localized Systems*; Y. Perlin, E., Wagner, M., Eds.; Elsevier: Amsterdam, 1984; pp 754.
(56) Garcia-Fernandez, P.; Trueba, A.; Barriuso, M. T.; Aramburu, J. A.; Moreno, M. Dynamic and Static Jahn-Teller Effect in Impurities: Determination of the Tunneling Splitting. In *Vibronic Interactions and the Jahn-Teller Effect*; Atanasov, M.; Daul, C.; Tregenna-Piggott, P., Eds.; Vibronic Interactions and the Jahn-Teller Effect. Progress in Theoretical Chemistry and Physics, vol *23*; Springer: Dordrecht, 2011; pp 105−142. DOI: DOI: 10.1007/978-94-007-2384-9_6.
(57) Palacio, F.; Morón, M. C. Magneto-Structural Correlations in Mn(III) Fluorides. In *Research Frontiers in Magneto Chemistry*; O'Connor, C. J., Ed.; World Scientific, 1993.
(58) Low, W.; Suss, J. T. Jahn-teller effect of Ni^{1+} and Cu^{2+} in single crystals of calcium oxide. *Phys. Lett.* **1963**, *7*, 310−312.
(59) Aramburu, J. A.; García-Fernández, P.; García-Lastra, J. M.; Moreno, M. A Genuine Jahn-Teller System with Compressed Geometry and Quantum Effects Originating from Zero-Point Motion. *ChemPhysChem* **2016**, *17*, 2146−2156.
(60) Riley, M. J.; Hitchman, M. A.; Reinen, D. Effects of vibronic coupling on the EPR spectra of copper(II) doped K_2ZnF_4. *Chem. Phys.* **1986**, *102*, 11−28.
(61) Aramburu, J. A.; García-Lastra, J. M.; García-Fernández, P.; Barriuso, M. T.; Moreno, M. Cu^{2+} in Layered Compounds: Origin of the Compressed Geometry in the Model System K_2ZnF_4:Cu^{2+}. *Inorg. Chem.* **2013**, *52*, 6923−6933.
(62) de Lucas, C. M.; Rodriguez, F.; Dance, J. M.; Moreno, M.; Tressaud, A. Luminescence of the new elpasolite Rb_2KGaF_6 doped with Cr^{3+}. *J. Lumin.* **1991**, *48-49*, 553−557.
(63) Hernández, I.; Rodríguez, F.; Tressaud, A. Optical Properties of the $(CrF_6)^{3-}$ Complex in A_2BMF_6:Cr^{3+} Elpasolite Crystals: Variation with M-F Bond Distance and Hydrostatic Pressure. *Inorg. Chem.* **2008**, *47*, 10288−10298.
(64) Babel, D.; Wall, F.; Heger, G. Die Kristall- und Magnetische Struktur von $CsFeF_4$. *Z. Naturforsch.* **1974**, *29b*, 139−148.
(65) Hidaka, M.; Fujii, H.; Garrard, B. J.; Wanklyn, B. M. Structural phase transitions in the layer compound $CsFeF_4$. *Phys. St. Solidi A* **1986**, *95*, 413−421.
(66) García-Lastra, J. M.; Aramburu, J. A.; Barriuso, M. T.; Moreno, M. Impurities in Noncubic Crystals: Stabilization Mechanisms for Jahn-Teller Ions in Layered Perovskites. *Phys. Rev. Lett.* **2004**, *93*, 226402.
(67) Bersuker, I. B.; Gorinchoi, N. N.; Polinger, V. Z. On the origin of dynamic instability of molecular systems. *Theor. Chim. Acta* **1984**, *66*, 161−172.
(68) Wingefeld, G.; Hoppe, R. Über $KCuAlF_6$. *Z. Anorg. Allg. Chem.* **1984**, *516*, 223−228.
(69) Finnie, K.; Dubicki, L.; Krausz, E. R.; Riley, M. J. Spectroscopic verification of a tetragonal compression in an octahedral copper(II) compound. *Inorg. Chem.* **1990**, *29*, 3908−3910.
(70) Aramburu, J. A.; Moreno, M. Ground State and Optical Excitations in Compounds with Tetragonal CuF_6^{4-} Units: Insight into $KAlCuF_6$ and $CuFAsF_6$. *Inorg. Chem.* **2020**, *59*, 539−547.
(71) Carrasco-Busturia, D.; Sánchez-Movellán, I.; Tygesen, A. S.; Bhowmik, A.; García-Lastra, J. M.; Aramburu, J. A.; Moreno, M. Red Shift in Optical Excitations on Layered Copper Perovskites under Pressure: Role of the Orthorhombic Instability. *Chem.—Eur. J.* **2023**, *29*, e202202933.
(72) Oelkrug, D. Absorption spectra and ligand field parameters of tetragonal 3d transition metal fluorides. *Struct. Bonding Berlin* **1971**, *9*, 1.
(73) Minner, E. M. C. Etude spectroscopique des ions Jahn-Teller cuivre et argent bivalents dans des monocristaux de fluoroperovskites de composition chimique AMF_3. Ph.D. Thesis, University of Geneva (Geneva), 1993.
(74) García-Fernández, P.; Barriuso, M. T.; García-Lastra, J. M.; Moreno, M.; Aramburu, J. A. Compounds Containing Tetragonal Cu^{2+} Complexes: Is the d_{x2-y2}-d_{3z2-r2} Gap a Direct Reflection of the Distortion? *J. Phys. Chem. Lett.* **2013**, *4*, 2385−2390.
(75) Dubicki, L.; Riley, M. J.; Krausz, E. R. Electronic structure of the copper(II) ion doped in cubic $KZnF_3$. *J. Chem. Phys.* **1994**, *101*, 1930−1939.
(76) Riley, M. J.; Dubicki, L.; Moran, G.; Krausz, E. R.; Yamada, I. Absorption and magnetic circular dichroism spectra of the compressed copper (II) ion in K_2ZnF_4. *Chem. Phys.* **1990**, *145*, 363−373.
(77) Riley, M. J.; Dubicki, L.; Moran, G.; Krausz, E. R.; Yamada, I. Optical spectrum of dipotassium tetrafluorocuprate. *Inorg. Chem.* **1990**, *29*, 1614−1626.
(78) Sánchez-Movellán, I.; Aramburu, J. A.; Moreno, M. Local structure and excitations in systems with CuF_6^{4-} units: lack of Jahn-Teller effect in the low symmetry compound Na_2CuF_4. *Phys. Chem. Chem. Phys.* **2020**, *22*, 7875−7887.
(79) De Jongh, L. J.; Block, R. On the exchange interactions in some 3d-metal ionic compounds: I. The 180° superexchange in the 3d-metal fluorides XMF_3 and X_2MF_4 (X = K, Rb, Tl; M = Mn, Co, Ni). *Physica B+C* **1975**, *79*, 568−593.
(80) Ishizuka, M.; Henmi, S.; Endo, S.; Moron, M. C.; Palacio, F. Magnetic behavior of $CsMnF_4$ under high pressure. *J. Magn. Magn. Mater.* **1999**, *196−197*, 440−442.
(81) Behatha, A.; Roy, A. J.; Anusree, C. V.; Ponvijayakanthan, L.; Sharma, V. K.; Kanchana, V. Correlation driven topological nodal ring ferromagnetic spin gapless semimetal: $CsMnF_4$. *J. Phys.: Condens. Matter* **2021**, *33*, 165803.

(82) Takeuchi, H.; Arakawa, M.; Aoki, H.; Yosida, T.; Horai, K. EPR and ^{19}F-ENDOR of Cr^{3+} Impurity Centres in K_2ZnF_4 and K_2MgF_4. *J. Phys. Soc. Jpn.* **1982**, *51*, 3166.
(83) García-Lastra, J. M.; Barriuso, M. T.; Aramburu, J. A.; Moreno, M. Cr^{3+} in layered perovskites: do the electron paramagnetic resonance parameters only depend on the impurity-ligand distances? *J. Phys.: Condens. Matter* **2010**, *22*, 155502.
(84) Gaăzo, J.; Bersuker, I. B.; Garaj, J.; Kabesova, M.; Kohout, J.; Langfelderova, H.; Melnik, M.; Serator, M.; Valach, F. Plasticity of the coordination sphere of copper(II) complexes, its manifestation and causes. *Coord. Chem. Rev.* **1976**, *19*, 253−297.
(85) Berke, H. The invention of blue and purple pigments in ancient times. *Chem. Soc. Rev.* **2007**, *36*, 15−30.
(86) García-Fernández, P.; Moreno, M.; Aramburu, J. A. Origin of the Exotic Blue Color of Copper-Containing Historical Pigments. *Inorg. Chem.* **2015**, *54*, 192−199.
(87) Moreno, M.; Barriuso, M. T.; Aramburu, J. A.; Garcia-Fernandez, P.; Garcia-Lastra, J. M. Microscopic insight into properties and electronic instabilities of impurities in cubic and lower symmetry insulators: the influence of pressure. *J. Phys.: Condens. Matter* **2006**, *18*, R315−R360.
(88) Bill, H. Observation of Cu^{2+} In $SrCl_2$ crystals. *Phys. Lett. A* **1973**, *44*, 101−102.
(89) García Fernández, P.; Aramburu, J. A.; Barriuso, M. T.; Moreno, M. Cu^{2+} impurities in fluorite-type crystals: Mechanisms favoring an off-center motion. *Phys. Rev. B* **2004**, *69*, 174110.

https://doi.org/10.1021/acs.inorgchem.4c00599
Inorg. Chem. 2024, 63, 13231−13243